Exceptionally deficient topological square-root insulators

Subhajyoti Bid and Henning Schomerus
Department of Physics, Lancaster University, Lancaster, LA1 4YB, United Kingdom
(Dated: January 26, 2026)

One of the most surprising features of effectively non-Hermitian physical systems is their potential to exhibit a striking nonlinear response and fragility to small perturbations. This feature arises from spectral singularities known as exceptional points, whose realization in the spectrum typically requires fine-tuning of parameters. The design of such systems receives significant impetus from the recent conception of *exceptional deficiency*, in which the entire energy spectrum is composed of exceptional points. Here, we present a concrete and transparent mechanism that enforces exceptional deficiency through lattice sum rules in non-Hermitian topological square-root insulators. We identify the resulting dynamical signatures in static broadband amplification and non-Abelian adiabatic state amplification, differentiate between bulk and boundary effects, and outline routes to implementation in physical platforms.

Effectively non-Hermitian physical systems can exhibit striking responses to small perturbations, a behavior rooted in spectral singularities known as exceptional points (EPs) [1–6]. At an EP, the eigenstates associated with the degenerate eigenvalue become identical, in contrast to the situation in Hermitian systems where the eigenstates form a basis. This eigenstate coalescence leads to dramatically altered static and dynamical responses to external perturbations [7, 8] and driving [9, 10] down to the quantum limit [11–13], which can be exploited, for instance, for sensing [14–20], lasing [21, 22], amplification [23, 24], and mode conversion [25, 26]. Realizing EPs typically requires fine-tuning, making their robust engineering a central challenge. The number of parameters required to obtain a single EP in the spectrum can be lowered by symmetries, such as parity-time symmetry in gain-loss balanced structures [27]. The realization of higher–order EPs, in which the number of coalescing states is larger than two, has benefitted from the introduction of non-reciprocal and unidirectional coupling schemes, which can be realized in topolectric [28, 29], mechanic [30–33], and quantum-optical [34] lattice systems as well as resonator-waveguide arrangements [35, 36]. Despite these advances, conventional EP implementations remain limited in scope: their functionality is typically restricted to narrow spectral regions near isolated EPs, and their realization often hinges on delicate parameter tuning or symmetry constraints that fix the position of the EP in the spectrum. This poses a fundamental limitation for broadband applications or robust device design. In light of this, the recently introduced concept of *exceptional deficiency* [37]—in which every energy level of a system is an exceptional point—marks a significant conceptual breakthrough. It opens the door to broadband EP-enhanced phenomena and offers a new route toward practical non-Hermitian functionalities. The original proposal, implemented in active mechanical lattices, achieves this through a tailored coupling between two subsystems with matching spectra.

Here, we present a concrete and transparent mechanism that enforces exceptional deficiency via lattice sum rules in non-Hermitian square-root topological insulators. The square-root construction principle [38] provides concrete guidance for the design and interpretation of a wide range of lattice systems with topological properties [39–45], including higher-order topological systems such as quadrupole insulators (QIs) [46, 47], which we will employ to illustrate our results. Applied to exceptional deficiency, this approach offers a natural path to identify two subsystems with matching spectra, provided by mutually coupled sublattices, as well as an explicit condition for the required coupling configuration. As square-root topological insulators offer a wide range of phenomena, they also present an ideal platform for identifying signatures of exceptional deficiency. We demonstrate this here for static broadband amplification and adiabatic state amplification, and show that this leads to state-selective and non-Abelian amplification mechanisms. Before we discuss these phenomena, we describe the general construction principle of exceptionally deficient topological square-root topological insulators and their implementation in the QI setting.

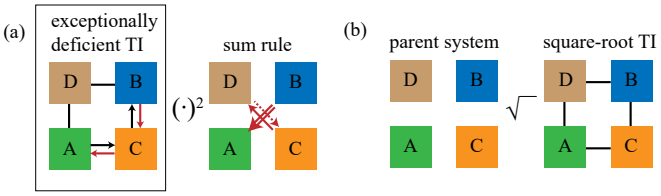

FIG. 1. (a) Construction principle of an exceptionally deficient topological insulator (TI) based on a sublattice sum rule inherited from a squared parent system. The sum rule constrains the nonreciprocal non-Hermitian couplings with part C (arrows) so that the squared parent system displays unidirectional couplings from subpart B to subpart A (double arrow). (b) Interpretation as a square-root TI, resulting in a nontrivial system with chiral symmetry.

Construction principle. Figure 1 depicts the general construction principle of exceptionally deficient topolog-

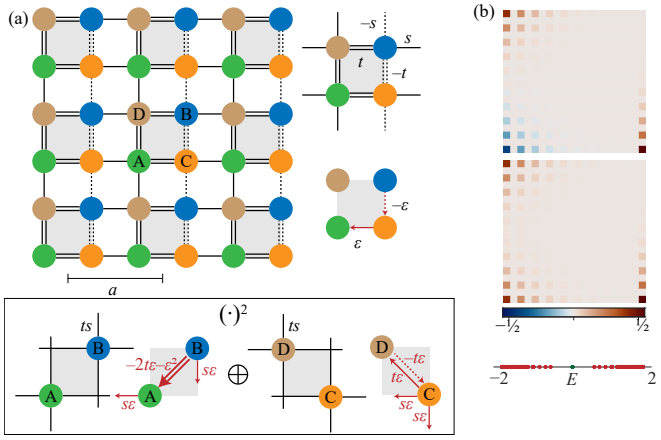

FIG. 2. (a) Implementation based on a π-flux quadrupole insulator with reciprocal couplings $s \equiv 1$ and t as well as additional nonreciprocal couplings of strength ε. The squared parent system (box) decomposes into the AB and CD subsystems, where the sum rule enforces unidirectional couplings between A and B. (b) The two corner states for the system in (a) with 10×10 unit cells and in $\varepsilon = -t = 1/2$. Each state belongs to two degenerate eigenvalues forming an exceptional point, and this also applies to all other states of this exceptionally deficient system. The bottom part shows the energy spectrum of the system, with the zero-energy corner states marked in green.

ical square-root insulators, along with a specific implementation based on a quadrupole insulator. The square-root construction connects uncoupled parent systems with Hamiltonian H^2 with a non-trivially coupled system with Hamiltonian H. In our example, the parent systems provide four sublattices, labelled A, B, C, and D, which are taken to be equivalent in the Hermitian limit. We consider nontrivial square roots that mutually couple sublattices (A,B) to sublattices (C,D), resulting in a generic block Hamiltonian

$$H = \begin{pmatrix} 0 & 0 & H_{AC} & H_{AD} \\ 0 & 0 & H_{BC} & H_{BD} \\ H_{CA} & H_{CB} & 0 & 0 \\ H_{DA} & H_{DB} & 0 & 0 \end{pmatrix} \tag{1}$$

possessing a chiral sublattice symmetry $\mathcal{X}H\mathcal{X} = -H$ with $\mathcal{X} = \mathrm{diag}(\mathbb{1}, \mathbb{1}, -\mathbb{1}, -\mathbb{1})$. Taking the couplings to be real, we also obtain a conventional time-reversal symmetry corresponding to complex conjugation $\mathcal{K}$. Exceptional deficiency will be enforced by demanding the lattice sum rule (lattice assignment without loss of generality)

$$H_{BC}H_{CA} + H_{BD}H_{DA} = 0, \tag{2}$$

and supplementing this with a generalized transposition symmetry [48, 49]

$$RH^TR = H, \quad R = \begin{pmatrix} 0 & \mathbb{1} & 0 & 0 \\ \mathbb{1} & 0 & 0 & 0 \\ 0 & 0 & -\mathbb{1} & 0 \\ 0 & 0 & 0 & \mathbb{1} \end{pmatrix}, \tag{3}$$

where the involution R, inherited from the sublattice permutation symmetry of the parent system, commutes with the chiral operator, $\mathcal{X}R\mathcal{X} = R$.

Given the sublattice sum rule (2), we can construct right eigenstates $\mathbf{u}_l = (\mathbf{a}_l, \mathbf{0}, \mathbf{c}_l, \mathbf{d}_l)^T$ (a column vector) by solving the reduced eigenvalue problem

$$(H_{AC}H_{CA} + H_{AD}H_{DA})\mathbf{a}_l = E_l^2\mathbf{a}_l \tag{4}$$

associated with the A sublattice of the parent system, choosing E_l as the positive or negative square root of E_l^2, and completing the eigenstate with $\mathbf{c}_l = E_l^{-1}H_{CA}\mathbf{a}_l$, $\mathbf{d}_l = E_l^{-1}H_{DA}\mathbf{a}_l$. Analogously, we obtain left eigenstates $\mathbf{v}_m = (\mathbf{0}, \mathbf{b}'_m, \mathbf{c}'_m, \mathbf{d}'_m)$ (a row vector) by solving the reduced eigenvalue problem

$$\mathbf{b}'_m(H_{BC}H_{CB} + H_{BD}H_{DB}) = E_m^2\mathbf{b}'_m \tag{5}$$

associated with the B sublattice of the parent system, choosing E_m as the positive or negative square root of E_m^2, and completing the eigenstate with $\mathbf{c}'_m = E_m^{-1}\mathbf{b}'_lH_{BC}$, $\mathbf{d}'_m = E_m^{-1}\mathbf{b}'_lH_{BD}$.

The sublattice sum rule (2) guarantees that

$$\mathbf{v}_m \cdot \mathbf{u}_l = 0, \tag{6}$$

and crucially this holds even when $E_l = E_m$. The generalized transposition symmetry transforms the reduced eigenvalue problems (4) and (5) into each other, so that the constructed right and left eigenstates can be paired up throughout the whole spectrum. In a Hermitian setting, where right and left eigenstates can furthermore be translated into each other, we have constructed a basis, and realize that all eigenvalues are even-fold degenerate, without resorting, for instance, to an explicit Kramers degeneracy [50, 51]. In generic non-Hermitian systems, however, the condition (6) amounts to self-orthogonality, which marks out EPs [1–5]. Thereby, we have constructed an exceptionally deficient system.

QI based realization. To illuminate how this construction results in exceptional deficiency, we turn to the concrete implementation given in Fig. 2(a). This implementation is based on a standard Hermitian QI model [46], formed by a unit cell with four sites, intracell couplings t, and intercell couplings $s \equiv 1$. The non-Hermitian modification is obtained from additional nonreciprocal intracell couplings of strength ε, while the topologically nontrivial features arise from π fluxes attached to each plaquette. The Hermitian system possesses a four-fold rotational symmetry induced by

$$C_4 = \begin{pmatrix} 0 & \mathbb{1} \\ -i\sigma_2 & 0 \end{pmatrix}, \tag{7}$$

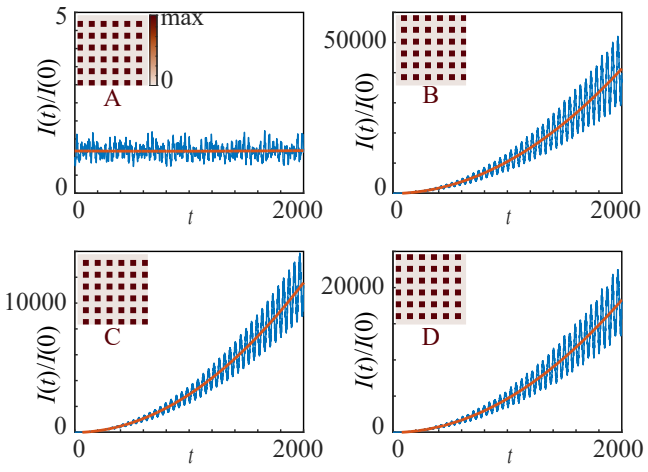

FIG. 3. Static state amplification in the exceptionally deficient QI with 6×6 unit cells and fixed $\varepsilon = 1/4$, $t = -1/2$. The insets show the intensity distribution of the chosen initial states, which are uniformly localized on the A, B, C, or D sublattices. The main panels display the time dependence of the total intensity. Significant state amplification $\propto t^2$ (red curves from polynomial fits) occurs whenever the initial state has components outside of the span of the eigenstates (the A sublattice lies within this span). This provides a broadband signature of exceptional deficiency.

with block Pauli matrices σ_i, where notably $C_4^4 = -\mathbb{1}$. The symmetries can further be combined into a generalized time-reversal symmetry operation $\mathcal{T} = \mathcal{K}C_4^2$, $\mathcal{T}^2 = -1$, rendering all energy levels in the Hermitian model two-fold Kramers degenerate. Importantly, the C_4 symmetry is broken in the non-reciprocal couplings of strength ε, and the system does not display non-Hermitian Kramers degeneracy [51]. Instead, the stated sum rule and generalized transposition symmetry enforce exceptional deficiency.

By construction of the model, these features apply to finite systems with open boundary conditions. In the range $|t| < 1$ the Hermitian QI then exhibits four corner states that appear in two-fold degenerate pairs at opposite energies close to zero. In the non-Hermitian model, these states instead form two EPs. We illustrate these corner states in Fig. 2 (b), where $\varepsilon = -t = 1/2$. Because of the exceptional deficiency, not only these corner states, but all size-quantized states in this finite system, are EPs. Next, we identify two dynamical signatures of the exceptional deficiency in such finite systems, obtained from the state evolution $i\frac{d}{dt}\boldsymbol{\psi}(t) = H(t)\boldsymbol{\psi}(t)$ with static or adiabatically time-dependent Hamiltonian $H(t)$.

Static broadband state amplification. For time-independent Hamiltonians H, the key dynamical signature of exceptional points is the occurrence of a solution $\exp(-iE_l t)\mathbf{w}_l - it\exp(-iE_l t)\mathbf{u}_l$ along with the standard solution $\exp(-iE_l t)\mathbf{u}_l$, where E_l is the degenerate eigenvalue, $\mathbf{u}_l$ the degenerate eigenvector, and $\mathbf{w}_l$ the generalized eigenvector obeying $H\mathbf{w}_l = E_l\mathbf{w}_l + \mathbf{u}_l$ [1]. The total intensity $I(t) = |\boldsymbol{\psi}(t)|^2$ then acquires a t^2 dependence, which is absent only when the initial state does not overlap with the generalized eigenvector. In an exceptionally deficient system, this static state amplification should occur for any initial condition that lies outside of the span of the eigenvectors $\mathbf{u}_l$, elevating it to a broadband effect. To obtain a clear signature of this broadband effect, we utilize the fact that in the QI realization, the A sublattice lies completely within the span of the eigenvectors, while the B sublattice lies completely outside this span. As shown in Fig. 3, the dynamical signatures are then directly observable in the time-dependent intensity from initial states that are uniformly distributed on a given sublattice [52]. As expected, state amplification is absent for the initial state on the A sublattice, but occurs for initial states localized on any of the three other sublattices, and it is most pronounced for the initial state on the B sublattice. In all these three cases, we observe a clear t^2 dependence, up to coherent periodic oscillations that generally depend on the initial state.

Non-Abelian adiabatic state amplification. Next, we utilize the corner states in the QI model to illuminate the dynamical consequences of the exceptional deficiency in a second setting. For this, we exploit the fact that the deficiency is maintained across the whole parameter range, which provides us with the opportunity to explore how states dynamically evolve while being stabilized at an EP. This feature leads us to consider the phenomenon of adiabatic state amplification [53–55], concerning the intensity change $I(t) = |\psi(t)|^2$ of a state as parameters $\boldsymbol{\lambda}$ are slowly changed along a path C. This effect is manifestly non-Hermitian, as Hermitian evolution preserves the norm of a state. Initialized in a long-living, spectrally isolated, right eigenstate $|R(\boldsymbol{\lambda}(0))\rangle$, with the long lifetime required so that the adiabatic theorem applies [56, 57], the state follows the instantaneous right eigenstate $|R(\boldsymbol{\lambda})\rangle$, while the intensity acquires a geometric amplification factor

$$A_g(C) = \exp\left[-2\int_C \mathrm{Im}\left[\boldsymbol{\mathcal{A}}^{LR}(\boldsymbol{\lambda}) - \boldsymbol{\mathcal{A}}^{RR}(\boldsymbol{\lambda})\right]\cdot d\boldsymbol{\lambda}\right] \quad (8)$$

connected with the imaginary part of the Berry connections

$$\boldsymbol{\mathcal{A}}^{LR}(\boldsymbol{\lambda}) = i\frac{\langle L(\boldsymbol{\lambda})|\nabla_{\boldsymbol{\lambda}} R(\boldsymbol{\lambda})\rangle}{\langle L(\boldsymbol{\lambda})|R(\boldsymbol{\lambda})\rangle}, \quad (9)$$

$$\boldsymbol{\mathcal{A}}^{RR}(\boldsymbol{\lambda}) = i\frac{\langle R(\boldsymbol{\lambda})|\nabla_{\boldsymbol{\lambda}} R(\boldsymbol{\lambda})\rangle}{\langle R(\boldsymbol{\lambda})|R(\boldsymbol{\lambda})\rangle}, \quad (10)$$

where $\langle L(\boldsymbol{\lambda})|$ is the associated instantaneous left eigenstate. As the intensity is a measurable physical quantity, the geometric amplification factor is gauge invariant even when the path C is open. On the other hand, expression (8) implies $A_g = 1$ for any closed path C that retraces itself back to the starting point, a feature tied to the Abelian nature of the associated complex Berry phase.

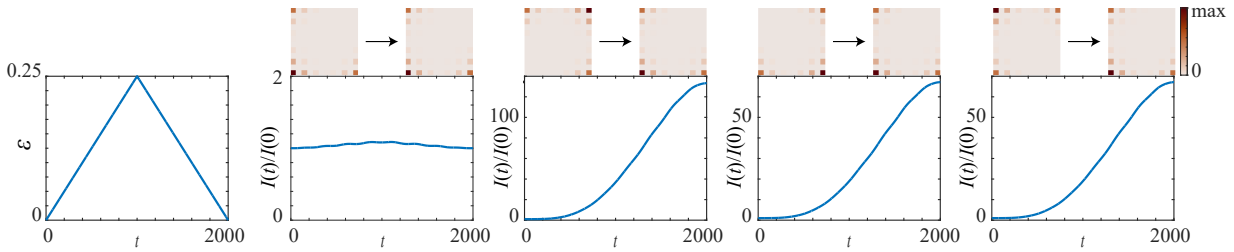

FIG. 4. Adiabatic state amplification in the exceptionally deficient QI with 6×6 unit cells and $t = -1/2$, as ε is ramped up and down. The insets show the chosen initial state (predominantly localized in one of the four corners) and the corresponding final state, which is always predominantly localized in the lower left corner. Significant state amplification $\propto (d\varepsilon/dt)^{-2}$ occurs whenever the initial state differs from this dynamically selected final state.

The Berry phase becomes non-Abelian when the state is degenerate [58], and in the non-Hermitian setting, this non-Abelian phase again acquires imaginary parts [59]. As shown in Fig. 4, concrete non-Abelian effects manifest for the exceptionally deficient non-Hermitian QI, making them directly observable in the state amplification. In the figure, we amplify a state by slowly varying ε over time from the Hermitian starting point $\varepsilon = 0$ to $\varepsilon = 1/4$, and then back to $\varepsilon = 0$. For the initial state we consider, in turn, one of the four corner states, predominantly localized on the A, B, C, or D sublattice (see insets). The first non-Abelian manifestation is the observation that at the end of the evolution, the final state has been transformed into the state predominately localized on the A sublattice. The second non-Abelian manifestation is the observation that, with the exception of the situation where the initial state is equal to this universal state, a significant intensity amplification has occurred. Notably, both effects occur even though the path C retraced itself, thus, would be absent in the Abelian case. The state amplification is systematic, scaling as $\sim (d\varepsilon/dt)^{-2}$ [60] in analogy with the t^2 scaling of static amplification described above, and is equal for the two evolutions starting predominantly on the C and D sublattices, while the amplification of the state starting on the B sublattice is twice as large.

Signatures of broken bulk-boundary correspondence. The dynamical effects described so far occur for finite systems, benefiting from the exactness of the described construction principle. However, the spectral features of non-Hermitian systems with non-reciprocal couplings are known to be highly sensitive to the boundary conditions, invalidating the bulk-boundary principle that connects finite and infinite periodic systems in Hermitian topology [61, 62]. This characteristic is exemplified by the non-Hermitian skin effect [63–67], where the bulk and boundary spectra for periodic and open boundary conditions drastically differ. In the described non-Hermitian QI model, we find that while states of the infinitely periodic system remain strictly degenerate, the degeneracies are no longer necessarily exceptional points, so that the system is only partially exceptionally deficient. This behavior follows directly from analyzing the Bloch Hamiltonian [52]

$$H(k_x,k_y)=\begin{pmatrix} 0 & 0 & r+e^{-ik_x} & t+e^{-ik_y} \\ 0 & 0 & -t-e^{ik_y} & t+e^{ik_x} \\ t+e^{ik_x} & -r-e^{-ik_y} & 0 & 0 \\ t+e^{ik_y} & t+e^{-ik_x} & 0 & 0 \end{pmatrix}, \tag{11}$$

where $r = t + \varepsilon$ and we set the lattice constant $a \equiv 1$. The sum rule (2) is obtained from the identity

$$(-t-e^{ik_y})(t+e^{ik_x})+(t+e^{ik_x})(t+e^{ik_y})=0, \tag{12}$$

highlighting the role of the π fluxes generated by the nontrivial square root. The generalized transposition symmetry takes the form

$$\begin{pmatrix} \sigma_1 & 0 \\ 0 & -\sigma_3 \end{pmatrix} H(k_x,k_y) \begin{pmatrix} \sigma_1 & 0 \\ 0 & -\sigma_3 \end{pmatrix} = H^T(k_y,k_x), \tag{13}$$

amounting to a reflection about the line $x+y=0$. Hence, the four bands

$$\begin{aligned} E^{(1)}_{\pm}(k_x,k_y) &= \pm\sqrt{|t+e^{ik_x}|^2+|t+e^{ik_y}|^2+\varepsilon(t+e^{ik_x})}, \\ E^{(2)}_{\pm}(k_x,k_y) &= \pm\sqrt{|t+e^{ik_x}|^2+|t+e^{ik_y}|^2+\varepsilon(t+e^{ik_y})}, \end{aligned} \tag{14}$$

whose winding in the complex plane signifies the non-Hermitian skin effect [67], respect the spectral symmetry $E^{(1)}_{\pm}(k_x,k_y) = E^{(2)}_{\pm}(k_y,k_x)$. For $k_x \neq k_y$, the band degeneracy occurs between different locations in the Brillouin zone, involving two mutually orthogonal extended Bloch states, as in a Kramers-degenerate system. Therefore, the continuous spectrum of this system exhibits exceptional deficiency only for $k_x = k_y \equiv k$, where each of the twofold degenerate bands $E^{(1)}_{+}(k,k) = E^{(2)}_{+}(k,k)$ and $E^{(1)}_{-}(k,k) = E^{(2)}_{-}(k,k)$ is associated with a unique extended Bloch eigenstate $\mathbf{u}_{\pm}(k,k)e^{ik(x+y)}$. The proposed construction principle of exceptionally deficient

models thus also opens up a new avenue for exploring the breakdown of the bulk-boundary correspondence in non-Hermitian systems.

Conclusions and outlook. In summary, we provided a transparent construction principle to design non-Hermitian systems that exhibit exceptional deficiency. The square root construction allowed us to equip the system with topological features, which we exemplified by a quadrupole insulator model with corner states. Exceptional deficiency gives rise to striking dynamical signatures, including in broadband and adiabatic state amplification, and unveils non-Abelian geometric characteristics that can be utilized for mode conversion. Our framework is readily implementable in existing platforms such as topolectric circuits [28, 29], active acoustic and mechanical metamaterials [30–33], and quantum-optical systems [68], including dissipative cold atom setups [34], only requiring rearrangement of components in previous setups to adapt the nonreciprocal couplings to the stated sum rule. Thereby, our work establishes a versatile route for designing exceptionally deficient systems that can be flexibly equipped with desired features, enabling new phenomena across a broad range of non-Hermitian settings.

This research was funded by EPSRC via Grant No. EP/W524438/1.

The data that support the findings of this work are openly available [69].

[1] T. Kato, *Perturbation Theory for Linear Operators*. (Springer, New York, 1966).

[2] C. Dembowski, H.-D. Gräf, H. L. Harney, A. Heine, W. D. Heiss, H. Rehfeld, and A. Richter, Experimental observation of the topological structure of exceptional points, Phys. Rev. Lett. **86**, 787 (2001).

[3] W. D. Heiss, Exceptional points of non-Hermitian operators, J. Phys. A **37**, 2455 (2004).

[4] M. V. Berry, Physics of Nonhermitian Degeneracies, Czech. J. Phys. **54**, 1039 (2004).

[5] W. D. Heiss, The physics of exceptional points, J. Phys. A **45**, 444016 (2012).

[6] M.-A. Miri and A. Alu, Exceptional points in optics and photonics, Science **363**, eaar7709 (2019).

[7] L. N. Trefethen, Computation of pseudospectra, Acta Numerica **8**, 247–295 (1999).

[8] J. Wiersig, Response strengths of open systems at exceptional points, Phys. Rev. Res. **4**, 023121 (2022).

[9] H. Schomerus, Nonreciprocal response theory of non-Hermitian mechanical metamaterials: Response phase transition from the skin effect of zero modes, Phys. Rev. Res. **2**, 013058 (2020).

[10] A. Hashemi, K. Busch, D. N. Christodoulides, S. K. Ozdemir, and R. El-Ganainy, Linear response theory of open systems with exceptional points, Nat. Commun. **13**, 3281 (2022).

[11] G. Yoo, H.-S. Sim, and H. Schomerus, Quantum noise and mode nonorthogonality in non-Hermitian PT-symmetric optical resonators, Phys. Rev. A **84**, 063833 (2011).

[12] K. Takata, K. Nozaki, E. Kuramochi, S. Matsuo, K. Takeda, T. Fujii, S. Kita, A. Shinya, and M. Notomi, Observing exceptional point degeneracy of radiation with electrically pumped photonic crystal coupled-nanocavity lasers, Optica **8**, 184 (2021).

[13] L. Simonson, S. K. Ozdemir, A. Eisfeld, A. Metelmann, and R. El-Ganainy, Nonuniversality of quantum noise in optical amplifiers operating at exceptional points, Phys. Rev. Res. **4**, 033226 (2022).

[14] J. Wiersig, Enhancing the sensitivity of frequency and energy splitting detection by using exceptional points: Application to microcavity sensors for single-particle detection, Phys. Rev. Lett. **112**, 203901 (2014).

[15] W. Chen, Ş. Kaya Özdemir, G. Zhao, J. Wiersig, and L. Yang, Exceptional points enhance sensing in an optical microcavity, Nature (London) **548**, 192 (2017).

[16] H. Hodaei, A. Hassan, S. Wittek, H. Carcia-Cracia, R. El-Ganainy, D. Christodoulides, and M. Khajavikhan, Enhanced sensitivity at higher-order exceptional points, Nature (London) **548**, 187 (2017).

[17] Z. Xiao, H. Li, T. Kottos, and A. Alù, Enhanced sensing and nondegraded thermal noise performance based on PT-symmetric electronic circuits with a sixth-order exceptional point, Phys. Rev. Lett. **123**, 213901 (2019).

[18] Y.-H. Lai, Y.-K. Lu, M.-G. Suh, Z. Yuan, and K. Vahala, Observation of the exceptional-point-enhanced Sagnac effect, Nature (London) **576**, 65 (2019).

[19] J. Wiersig, Prospects and fundamental limits in exceptional point-based sensing, Nat. Commun. **11**, 2454 (2020).

[20] R. Kononchuk, J. Cai, F. Ellis, R. Thevamaran, and T. Kottos, Exceptional-point-based accelerometers with enhanced signal-to-noise ratio, Nature (London) **607**, 697 (2022).

[21] B. Peng, Şahin Kaya Özdemir, M. Liertzer, W. Chen, J. Kramer, H. Yılmaz, J. Wiersig, S. Rotter, and L. Yang, Chiral modes and directional lasing at exceptional points, PNAS **113**, 6845 (2016).

[22] P. Miao, Z. Zhang, J. Sun, W. Walasik, S. Longhi, N. M. Litchinitser, and L. Feng, Orbital angular momentum microlaser, Science **353**, 464 (2016).

[23] M. Zhang, W. Sweeney, C. W. Hsu, L. Yang, A. D. Stone, and L. Jiang, Quantum noise theory of exceptional point amplifying sensors, Phys. Rev. Lett. **123**, 180501 (2019).

[24] Q. Zhong, Ş. K. Özdemir, A. Eisfeld, A. Metelmann, and R. El-Ganainy, Exceptional points-based optical amplifiers, Phys. Rev. Appl. **13**, 014070 (2020).

[25] H. Xu, D. Mason, L. Jiang, and J. G. E. Harris, Topological energy transfer in an optomechanical system with exceptional points, Nature (London) **537**, 80 (2016).

[26] J. Doppler, A. A. Mailybaev, J. Böhm, U. Kuhl, A. Girschik, F. Libisch, T. J. Milburn, P. Rabl, N. Moiseyev, and S. Rotter, Dynamically encircling an exceptional point for asymmetric mode switching, Nature (London) **537**, 76 (2016).

[27] R. El-Ganainy, K. G. Makris, M. Khajavikhan, Z. H. Musslimani, S. Rotter, and D. N. Christodoulides, Non-Hermitian physics and PT symmetry, Nat. Phys. **14**, 11 (2018).

[28] T. Helbig, T. Hofmann, S. Imhof, M. Abdelghany, T. Kiessling, L. Molenkamp, C. Lee, A. Szameit, M. Greiter, and R. Thomale, Generalized bulk–boundary corre-

spondence in non-Hermitian topolectrical circuits, Nat. Phys. **16**, 747 (2020).
[29] D. Zou, T. Chen, W. He, J. Bao, C. H. Lee, H. Sun, and X. Zhang, Observation of hybrid higher-order skin-topological effect in non-Hermitian topolectrical circuits, Nat. Commun. **12**, 7201 (2021).
[30] M. Brandenbourger, X. Locsin, E. Lerner, and C. Coulais, Non-reciprocal robotic metamaterials, Nat. Commun. **10**, 4608 (2019).
[31] A. Ghatak, M. Brandenbourger, J. Van Wezel, and C. Coulais, Observation of non-Hermitian topology and its bulk–edge correspondence in an active mechanical metamaterial, PNAS **117**, 29561 (2020).
[32] X. Zhang, Y. Tian, J.-H. Jiang, M.-H. Lu, and Y.-F. Chen, Observation of higher-order non-Hermitian skin effect, Nat. Commun. **12**, 5377 (2021).
[33] J. Veenstra, O. Gamayun, X. Guo, A. Sarvi, C. V. Meinersen, and C. Coulais, Non-reciprocal topological solitons in active metamaterials, Nature (London) **627**, 528 (2024).
[34] Q. Liang, D. Xie, Z. Dong, H. Li, H. Li, B. Gadway, W. Yi, and B. Yan, Dynamic signatures of non-Hermitian skin effect and topology in ultracold atoms, Phys. Rev. Lett. **129**, 070401 (2022).
[35] J. Kullig, D. Grom, S. Klembt, and J. Wiersig, Higher-order exceptional points in waveguide-coupled microcavities: Perturbation induced frequency splittings and mode patterns, Photonics Res. **11**, A54 (2023).
[36] S. Soleymani, Q. Zhong, M. Mokim, S. Rotter, R. El-Ganainy, and Ş. K. Özdemir, Chiral and degenerate perfect absorption on exceptional surfaces, Nat. Commun. **13**, 599 (2022).
[37] Z. Li, X. Wang, R. Cai, K. Shimomura, Z. Yang, M. Sato, and G. Ma, Exceptional deficiency of non-Hermitian systems: high-dimensional coalescence and dynamics, arXiv (2025), arXiv:2504.12238 [quant-ph].
[38] J. Arkinstall, M. H. Teimourpour, L. Feng, R. El-Ganainy, and H. Schomerus, Topological tight-binding models from nontrivial square roots, Phys. Rev. B **95**, 165109 (2017).
[39] M. Ezawa, Systematic construction of square-root topological insulators and superconductors, Phys. Rev. Res. **2**, 033397 (2020).
[40] M. Kremer, I. Petrides, E. Meyer, M. Heinrich, O. Zilberberg, and A. Szameit, A square-root topological insulator with non-quantized indices realized with photonic Aharonov-Bohm cages, Nat. Commun. **11**, 907 (2020).
[41] R. G. Dias and A. M. Marques, Matryoshka approach to sine-cosine topological models, Phys. Rev. B **103**, 245112 (2021).
[42] T. Mizoguchi, T. Yoshida, and Y. Hatsugai, Square-root topological semimetals, Phys. Rev. B **103**, 045136 (2021).
[43] L. Song, H. Yang, Y. Cao, and P. Yan, Square-root higher-order Weyl semimetals, Nat. Commun. **13**, 5601 (2022).
[44] A. M. Marques, J. Mögerle, G. Pelegrí, S. Flannigan, R. G. Dias, and A. J. Daley, Kaleidoscopes of hofstadter butterflies and Aharonov-Bohm caging from 2^n-root topology in decorated square lattices, Phys. Rev. Res. **5**, 023110 (2023).
[45] K. Roychowdhury, J. Attig, S. Trebst, and M. J. Lawler, Supersymmetry on the lattice: Geometry, topology, and flat bands, Phys. Rev. Res. **6**, 043273 (2024).
[46] W. A. Benalcazar, B. A. Bernevig, and T. L. Hughes, Quantized electric multipole insulators, Science **357**, 61 (2017).
[47] W. A. Benalcazar, B. A. Bernevig, and T. L. Hughes, Electric multipole moments, topological multipole moment pumping, and chiral hinge states in crystalline insulators, Phys. Rev. B **96**, 245115 (2017).
[48] H. Schomerus, From scattering theory to complex wave dynamics in non-Hermitian PT-symmetric resonators, Philos. Trans. R. Soc. A **371**, 20120194 (2013).
[49] N. Okuma, K. Kawabata, K. Shiozaki, and M. Sato, Topological origin of non-Hermitian skin effects, Phys. Rev. Lett. **124**, 086801 (2020).
[50] C. W. J. Beenakker, Random-matrix theory of quantum transport, Rev. Mod. Phys. **69**, 731 (1997).
[51] K. Esaki, M. Sato, K. Hasebe, and M. Kohmoto, Edge states and topological phases in non-Hermitian systems, Phys. Rev. B **84**, 205128 (2011).
[52] See Supplemental Material at `https://journals.aps.org/prr/supplemental/10.1103/PhysRevRes.XXX.XXXXX` for a detailed description of the bulk Hamiltonian as well as further numerical results.
[53] N. Silberstein, J. Behrends, M. Goldstein, and R. Ilan, Berry connection induced anomalous wave-packet dynamics in non-Hermitian systems, Phys. Rev. B **102**, 245147 (2020).
[54] Y. Singhal, E. Martello, S. Agrawal, T. Ozawa, H. Price, and B. Gadway, Measuring the adiabatic non-Hermitian Berry phase in feedback-coupled oscillators, Phys. Rev. Res. **5**, L032026 (2023).
[55] T. Ozawa and H. Schomerus, Geometric contribution to adiabatic amplification in non-Hermitian systems, Phys. Rev. Res. **7**, 013173 (2025).
[56] G. Nenciu and G. Rasche, On the adiabatic theorem for nonself-adjoint Hamiltonians, J. Phys. A **25**, 5741 (1992).
[57] E.-M. Graefe, A. A. Mailybaev, and N. Moiseyev, Breakdown of adiabatic transfer of light in waveguides in the presence of absorption, Phys. Rev. A **88**, 033842 (2013).
[58] F. Wilczek and A. Zee, Appearance of Gauge Structure in Simple Dynamical Systems, Phys. Rev. Lett. **52**, 2111 (1984).
[59] K. Snizhko, R. Egger, and Y. Gefen, Non-Abelian Berry phase for open quantum systems: Topological protection versus geometric dephasing, Phys. Rev. B **100**, 085303 (2019).
[60] J. Höller, N. Read, and J. G. E. Harris, Non-Hermitian adiabatic transport in spaces of exceptional points, Phys. Rev. A **102**, 032216 (2020).
[61] M. Z. Hasan and C. L. Kane, Colloquium: Topological insulators, Rev. Mod. Phys. **82**, 3045 (2010).
[62] X.-L. Qi and S.-C. Zhang, Topological insulators and superconductors, Rev. Mod. Phys. **83**, 1057 (2011).
[63] S. Yao and Z. Wang, Edge states and topological invariants of non-Hermitian systems, Phys. Rev. Lett. **121**, 086803 (2018).
[64] F. K. Kunst, E. Edvardsson, J. C. Budich, and E. J. Bergholtz, Biorthogonal bulk-boundary correspondence in non-Hermitian systems, Phys. Rev. Lett. **121**, 026808 (2018).
[65] K. Yokomizo and S. Murakami, Non-Bloch band theory of non-Hermitian systems, Phys. Rev. Lett. **123**, 066404 (2019).
[66] C. H. Lee and R. Thomale, Anatomy of skin modes and topology in non-Hermitian systems, Phys. Rev. B **99**,

201103 (2019).
[67] K. Zhang, Z. Yang, and C. Fang, Correspondence between winding numbers and skin modes in non-Hermitian systems, Phys. Rev. Lett. **125**, 126402 (2020).
[68] C. C. Wanjura, M. Brunelli, and A. Nunnenkamp, Topological framework for directional amplification in driven-dissipative cavity arrays, Nat. Commun. **11**, 3149 (2020).
[69] Research datasets at https://doi.org/10.5281/zenodo.16540598.

SUPPLEMENTARY MATERIAL: Exceptionally deficient topological square-root insulators

Subhajyoti Bid and Henning Schomerus
Department of Physics, Lancaster University, Lancaster, LA1 4YB, United Kingdom

SPECTRAL DEGENERACIES IN THE BLOCH HAMILTONIAN

In the main text we remarked that the infinite periodic counterpart of the designed exceptionally deficient squsre-rrot insulator displays exceptional points (EPs) only for $k_x = k_y$. Here we provide further details on the emergence of these EPs, and contrast these with the degeneracy of the original Hermitian quadrupole insulator (QI).

Kramers degeneracy in the Hermitian QI model

We start with the Hermitian QI model [1, 2], accounting for all its symmetries. The Bloch Hamiltonian of this model is given by

$$H_{\rm QI}(k_x,k_y) = \begin{pmatrix} 0 & 0 & t+e^{-ik_x} & t+e^{-ik_y} \\ 0 & 0 & -t-e^{ik_y} & t+e^{ik_x} \\ t+e^{ik_x} & -t-e^{-ik_y} & 0 & 0 \\ t+e^{ik_y} & t+e^{-ik_x} & 0 & 0 \end{pmatrix}, \tag{S1}$$

where we set the intercell coupling $s \equiv 1$. The model exhibits spinless time-reversal symmetry

$$\mathcal{T} H_{\rm QI}(k_x,k_y)\mathcal{T}^{-1} = H_{\rm QI}(-k_x,-k_y) \tag{S2}$$

where $\mathcal{T} = \mathcal{K}$ corresponds to complex conjugation, and respects a fourfold rotational

$$C_4\, H_{\rm QI}(k_x,k_y)\, C_4^{-1} = H_{\rm QI}(k_y,-k_x), \tag{S3}$$

where the transformation matrix

$$C_4 = \begin{pmatrix} 0 & \mathbb{1}_2 \\ -i\sigma_2 & 0 \end{pmatrix} \tag{S4}$$

fulfills $C_4^4 = -\mathbb{1}$, a feature induced by the π fluxes in all plaquettes. The Bloch Hamiltonian also possesses an intrinsic chiral symmetry arising from the bipartite nature of the lattice,

$$\mathcal{X}\, H_{\rm QI}(k_x,k_y)\, \mathcal{X} = -H_{\rm QI}(k_x,k_y), \tag{S5}$$

where the chiral operator

$$\mathcal{X} = \begin{pmatrix} \mathbb{1}_2 & 0 \\ 0 & -\mathbb{1}_2 \end{pmatrix} \tag{S6}$$

is traceless, reflecting the equal number of sites belonging to the two sublattices within each unit cell.

Upon diagonalizing the Hamiltonian in Eq. (S1), the energy dispersion takes the form

$$E_\pm(k_x,k_y) = \pm\sqrt{2[1+t^2+t(\cos k_x+\cos k_y)]}, \tag{S7}$$

where each band is twofold degenerate. This degeneracy can be attributed to the presence of a generalized time-reversal symmetry $\mathcal{T}' \equiv \mathcal{K}C_4^2$, fulfilling

$$\mathcal{T}' H_{\rm QI}(k_x,k_y)\mathcal{T}'^{-1} = H_{\rm QI}(k_x,k_y), \tag{S8}$$

and thereby constraining the Bloch Hamiltonian for any fixed quasimomenta k_x, k_y. As $\mathcal{T}'^2 = -\mathbb{1}$, this results in the formation of Kramers degenerate pairs across the entire Brillouin zone.

This interpretation is significantly simplified by interpreting the system as a square-root insulator. The squared Hermitian Bloch Hamiltonian takes a simple diagonal form [3]

$$H_{\rm QI}^2(k_x,k_y) = E^2(k_x,k_y)\,\mathbb{1}, \tag{S9}$$

which signifies that the four sublattices in the squared system are completely decoupled.

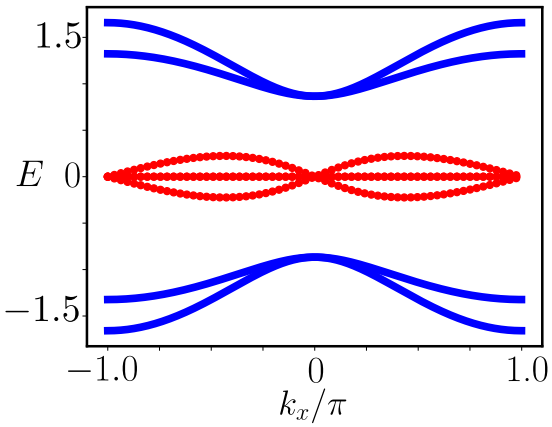

FIG. S1. Energy bands for the infinitely periodic counterpart of the exceptionally deficient QI model, with Bloch Hamiltonian (S10), as a function of k_x with fixed $k_y = 0$ (real part in blue, imaginary part dotted in red). The energy bands follow from the analytic expressions in Eq. (S14), where the parameters $\varepsilon = -t = 1/2$ are the same as those in Fig. 2 of the main text. On the symmetry line $k_x = k_y$, the four dispersion branches coallesce in two EPs.

Formation of EPs in the non-Hermitian model

With these preparations, we now describe the key modifications of the symmetries and degeneracy in the non-Hermitian model. For convenience, we reproduce the Bloch Hamiltonian of the non-Hermitian model [Eq. (11) in the main text],

$$H(k_x,k_y) = \begin{pmatrix} 0 & 0 & r+e^{-ik_x} & t+e^{-ik_y} \\ 0 & 0 & -t-e^{ik_y} & t+e^{ik_x} \\ t+e^{ik_x} & -r-e^{-ik_y} & 0 & 0 \\ t+e^{ik_y} & t+e^{-ik_x} & 0 & 0 \end{pmatrix} \tag{S10}$$

with $r = t+\varepsilon$. The model exhibits the conventional time-reversal symmetry $\mathcal{T}$ and chiral symmetry $\mathcal{X}$, but breaks the rotational symmetry C_4. Furthermore, the generalized time-reversal symmetry $\mathcal{T}'$ becomes reduced to the generalized transposition symmetry

$$\begin{pmatrix} \sigma_1 & 0 \\ 0 & -\sigma_3 \end{pmatrix} H(k_x,k_y) \begin{pmatrix} \sigma_1 & 0 \\ 0 & -\sigma_3 \end{pmatrix} = H^T(k_y,k_x), \tag{S11}$$

given as Eq. (13) in the main text. Importantly, in contrast to Eq. (S8), this generalized transposition symmetry constrains the Bloch Hamiltonian only for coinciding quasimomenta $k_x = k_y$.

To analyze the implications for the spectral degeneracy, we again study the squared parent Hamiltonian. This parent Hamiltonian takes the block-diagonal form

$$H^2(k_x,k_y) = \begin{pmatrix} H_I & 0 \\ 0 & H_{II} \end{pmatrix}, \tag{S12}$$

where the upper block

$$H_I = \begin{pmatrix} E_1^2(k_x,k_y,\varepsilon) & -\varepsilon\left(e^{-\mathrm{i}k_x}+e^{-\mathrm{i}k_y}+2t+\varepsilon\right) \\ 0 & E_2^2(k_x,k_y,\varepsilon) \end{pmatrix} \tag{S13}$$

contains the squared dispersions relations

$$\begin{aligned} E_1^2(k_x,k_y,\varepsilon) &= |t+e^{ik_x}|^2 + |t+e^{ik_y}|^2 + \varepsilon(t+e^{ik_x}), \\ E_2^2(k_x,k_y,\varepsilon) &= |t+e^{ik_x}|^2 + |t+e^{ik_y}|^2 + \varepsilon(t+e^{ik_y}) \end{aligned} \tag{S14}$$

of the non-Hermitian QI on its diagonals, in agreement with Eq. (14) of the main text. The lower block

$$H_{II} = \begin{pmatrix} 2t^2+2t\epsilon+2+(2t+\epsilon)(\cos k_x+\cos k_y)+i\epsilon(\sin k_x+\sin k_y) & -\epsilon(t+e^{ik_x}) \\ \epsilon(t+e^{ik_y}) & 2t^2+2+2t(\cos k_x+\cos k_y) \end{pmatrix} \tag{S15}$$

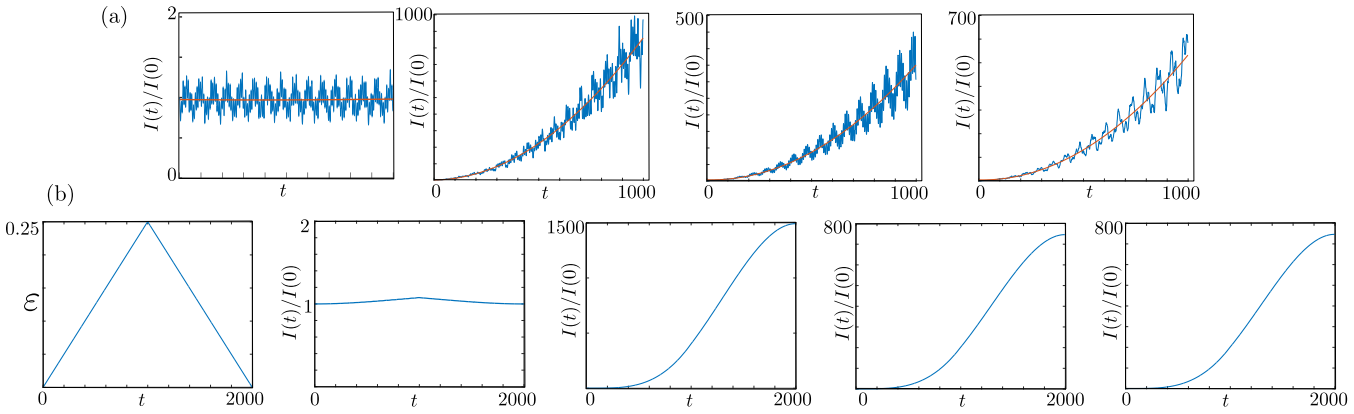

FIG. S2. Static state amplification (a) and adiabatic state amplification (b) for a reduced system size (4 × 4 unit cells) of the exceptionally deficient QI in panel, computed using the same parameter values and initial conditions as in the main text (cf. Figs. 3 and 4 of the main text).

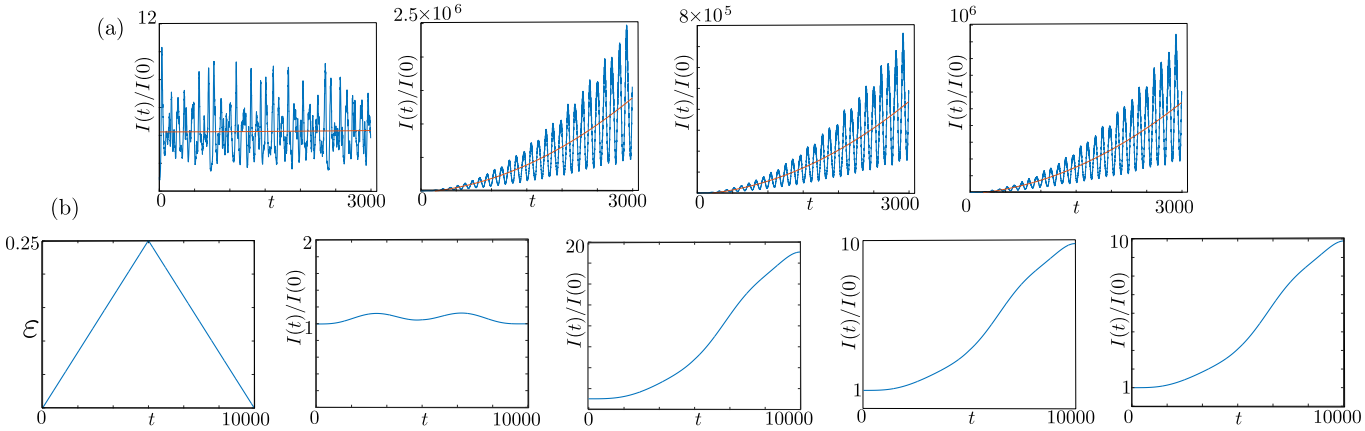

FIG. S3. Analogous to Fig. S2, but for a system of 10 × 10 unit cells.

delivers, by construction, the same energy spectrum. The upper triangular form of H_I is a direct consequence of the sublattice sum rule (2) of the main text, which in this specific case takes the form of Eq. (12) of the main text. We now note that at fixed k_x and k_y, the two squared dispersion branches coincide only when these satisfy $k_x = k_y$. Because of the upper triangular form of H_I, the eigensystem is then furthermore defective, so that the degeneracies along this symmetry line correspond to EPs. For $k_x \neq k_y$, we still observe degeneracy in the form $E_1^2(k_x, k_y, \varepsilon) = E_2^2(k_y, k_x, \varepsilon)$. However, this then connects Bloch wave functions with differing quasimomenta, hence, mutually orthogonal plane-wave components $\exp(ik_x x + ik_y y)$. In line with this, H_I is then no longer defective.

For further illustration, we depict in Fig. S1 the band structure of the system as a function of k_x with fixed $k_y = 0$, displaying the two EPs at $k_x = 0$.

ADDITIONAL NUMERICAL RESULTS AND EXPERIMENTAL CONSIDERATIONS

For further illustration of the signatures of exceptional deficiency, we here provide additional numerical results for smaller and larger system sizes (Figs. S2 and S3, as well as systems with reduced non-Hermiticity parameters and disorder (Figs. S4 and S5). In the latter case, we perturbed all Hermitian and non-Hermitian couplings with relative disorder drawn from a box distribution of width $W = 10^{-3}$, thereby breaking the sum rule and all symmetries, and lifting the exact exceptional deficiency. Ref. [4] establishes that exceptionally deficient systems behave predictably against such indiscriminate disorder, where in particular, the overlap of eigenspaces from two different sectors of the off-diagonal Hamiltonian remains large. The figure verifies numerically that these mathematical features also carry over to the practically observable amplification mechanisms.

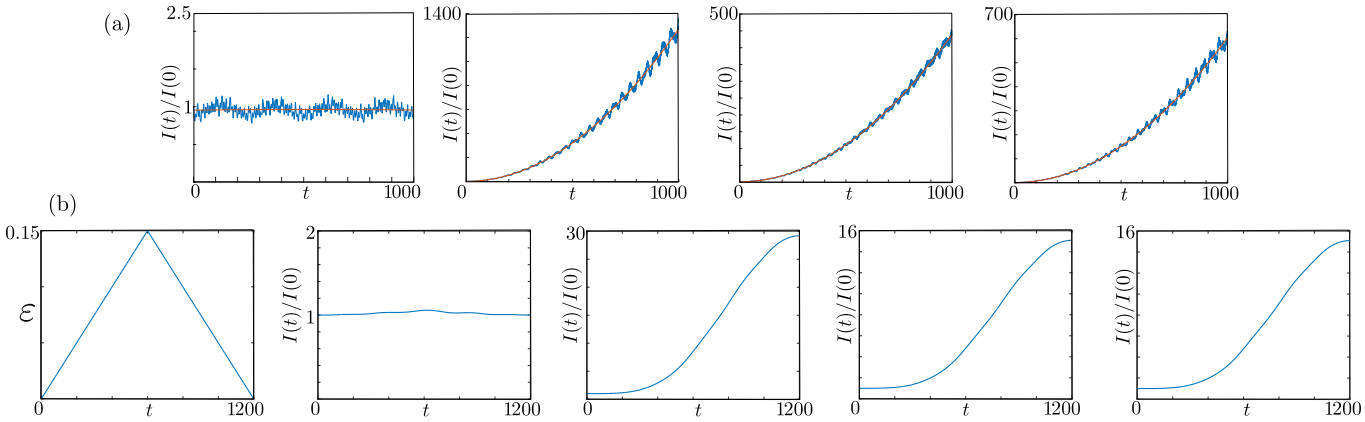

FIG. S4. Analogous to Fig. S2, but for a system of 6×6 unit cells with reduced non-Hermiticity parameter $\varepsilon = 0.15$.

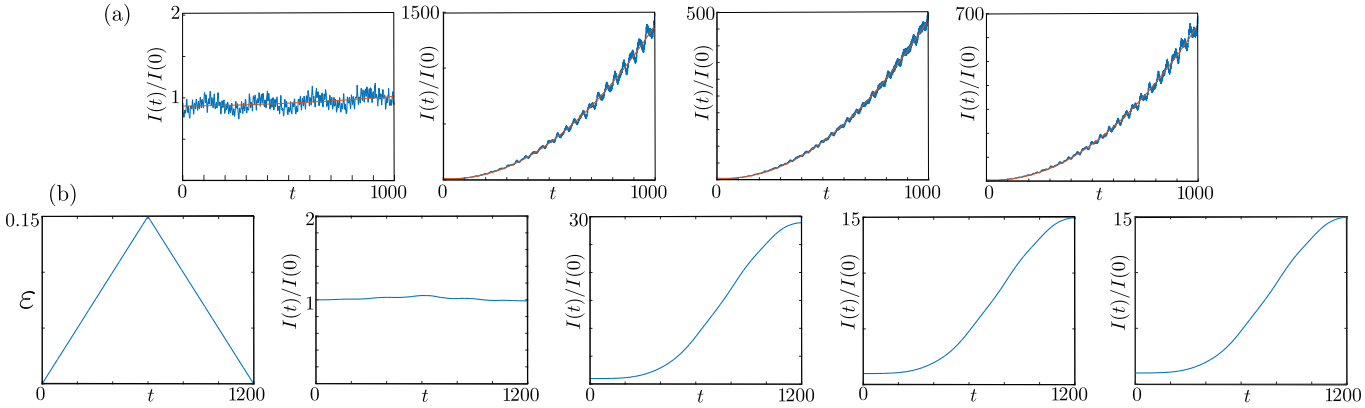

FIG. S5. Analogous to Fig. S4, but in presence of disorder, where all Hermitian and non-Hermitian couplings are independently perturbed by a relative disorder drawn from a box distribution of width $W = 10^{-3}$.

[1] W. A. Benalcazar, B. A. Bernevig, and T. L. Hughes, Quantized electric multipole insulators, Science **357**, 61 (2017).

[2] W. A. Benalcazar, B. A. Bernevig, and T. L. Hughes, Electric multipole moments, topological multipole moment pumping, and chiral hinge states in crystalline insulators, Phys. Rev. B **96**, 245115 (2017).

[3] J. Arkinstall, M. H. Teimourpour, L. Feng, R. El-Ganainy, and H. Schomerus, Topological tight-binding models from nontrivial square roots, Phys. Rev. B **95**, 165109 (2017).

[4] Z. Li, X. Wang, R. Cai, K. Shimomura, Z. Yang, M. Sato, and G. Ma, Exceptional deficiency of non-Hermitian systems: high-dimensional coalescence and dynamics, arXiv (2025), arXiv:2504.12238 [quant-ph].